Optics & Laser Technology 136 (2021) 106742

Contents lists available at ScienceDirect

Optics and Laser Technology

journal homepage: www.elsevier.com/locate/optlastec

Full length article

Transparent glass-ceramic waveguides made by femtosecond laser writing

P.H.D. Ferreira [a,*], D.C.N. Fabris [b], M.O.C. Villas Boas [b], I.G. Bezerra [a], C.R. Mendonça [c], E. D. Zanotto [b]

[a] Physics Department, Federal University of São Carlos, São Carlos 13565-905, SP, Brazil
[b] Graduate Program in Materials Science and Engineering, Federal University of Sao Carlos, 13565-905 São Carlos, SP, Brazil
[c] São Carlos Institute of Physics, University of São Paulo, PO Box 369, 13561-970 São Carlos, SP, Brazil

ARTICLE INFO

Keywords:
Femtosecond laser writing
Transparent glass-ceramic
Optical waveguide
Strengthened photonic device

ABSTRACT

Transparent glass-ceramics (TGC) have been investigated to replace hard, mechanically strong, scratch resistant materials in ballistic armor applications and smart phone displays. Certain types of TGC have superior performance than borosilicate and soda-lime glasses, and are much easier to produce, especially large parts, than transparent mono or polycrystalline ceramics. Thereupon, transparent glass-ceramics could be feasible in other applications, such as stronger photonic devices. In this work, we used femtosecond laser pulses to inscribe optical waveguides inside a magnesium aluminum silicate (MAS) precursor glass and glass-ceramic, which has shown satisfactory mechanical properties to be applied as ballistic armor. Single mode waveguides for the precursor glass and ring mode for MAS-TGC were obtained and characterized (total insertion loss, mode profile, and threshold energy for heat diffusion at different fabrication depths). Micro-Raman measurements on the micro-fabricated waveguide core and on the pristine material surface show some difference for the TGC, but none for the glass. Particularly, we found that the threshold energy for heat diffusion is higher in the MAS glass-ceramic than in its parent glass. Its good optical waveguiding and mechanical properties indicate that this new TGC might be adequate for photonic devices that require mechanically competent materials.

1. Introduction

In the last few years, transparent glass-ceramics (TGC) have attracted significant attention due to several compelling properties, which render then applicable, e.g., as armor materials [1,2]. Specifically in security applications, such as ballistic resistant windows, helmet visors and vehicles, due to their processing flexibility in fabricating large size samples and cost-effectiveness, they have been studied to replace other hard transparent materials, such as sapphire, aluminum oxynitride (AlON), and polycrystalline magnesium aluminate transparent ceramics [3]. However, glass-ceramics [4], which are multiple-phase nanocomposite materials constituted by nano or microcrystals embedded in a glass matrix [5], can also be investigated for other purposes, such as strengthened photonic devices. Glass-ceramics have much better performance than borosilicate and soda-lime glasses, being generally harder, stiffer, tougher, and stronger, and are much easier to produce than transparent ceramics, especially large parts [6]. Additionally, their properties can be functionalized by controlling the type, size distribution and volume fraction of the crystalline phase [1]. Among these properties, optical transparency is crucial in particular for use in optics and photonics, such as dielectric optical waveguides, windows and lasers, and many researches have been devoted to this topic [7,8].

Concomitantly, there has been growing attention on methods to process materials for the development of devices for use in several fields, from quantum computing [9] to biological sensing [10]. Femtosecond laser (fs-laser) micromachining has prompted as a potential approach in this direction, enabling the production of several optical devices, from gratings and interferometers to amplifiers, switches and waveguide couplers [11–18] (2). This technique has various advantages when compared to other methods, such as photolithography, high-energy ion implantation, and reactive ion etching [19]. The latter approaches often need prior design and fabrication of masks, demand many processing steps and are intrinsically planar technologies, while fs-laser fabrication allows single-step, maskless, direct processing [19–22]. Furthermore, micromachining with fs-laser pulses allows the production of 3D micro- and nano-structures [23].

In this work, straight waveguides were directly inscribed by femtosecond laser writing in the bulk of a magnesium aluminum silicate

* Corresponding author.
E-mail address: paulohdf@ufscar.br (P.H.D. Ferreira).

https://doi.org/10.1016/j.optlastec.2020.106742
Received 23 September 2020; Received in revised form 26 October 2020; Accepted 9 November 2020
Available online 1 December 2020

(MAS) glass-ceramic, which had shown satisfactory mechanical properties to be used as transparent armor window, and in the interior of the MAS parent glass, i.e., before the nucleation and crystal growth treatments.

The laser pulses (50-fs, 800-nm, and 5.2 MHz repetition rate) were tightly focused by a 40X objective inside the sample, which was moved using a translation stage. The resulting high-quality optical waveguides were characterized by total insertion loss, mode profile, threshold energy for heat diffusion at different fabrication depths and μ-Raman spectra. Moreover, the MAS TGC was characterized by X-ray diffraction and transmission electron microscopy. Additionally, both MAS TGC and glass optical transmittance were measured.

2. Materials and methods

To produce the glass and glass-ceramic, >99% purity chemicals were used: SiO_2 (Zetasil 4, Vitrovita), Al_2O_3 (Almatis), MgO (Sigma Aldrich) and ZrO_2 (Alfa Aesar), were mixed for 3 h using a powder mixer. The batch mixture of 150 g was placed in a covered-platinum crucible and melted at 1580–1630 °C. Then the viscous liquid was cast onto a metallic plate, ground and re-melted to increase the chemical homogeneity. This procedure was repeated 3 times. Finally, the melt was kept at the maximum temperature during 4 h, and cast in molds of approximately 1.5 × 1.5 × 5.5 cm. The pieces were annealed at ~35 °C below the glass transition temperature (T_g) to eliminate residual stresses. The glass transition temperature, T_g, is 830 °C, determined in a previous work. Then the muffle was switched-off and the glass was allowed to cool down to room temperature at a rate of approximately 3 K/min. The intended nanostructured glass–ceramic pieces were produced using a nucleation treatment at 830 °C for 14 days and crystal growth during 3 h at 1015 °C. This treatment schedule was found after several trials.

The monolithic solid material was cut in pieces of 10 × 3 × 2 mm^3 and polished using a wax base. Fig. 1 shows the TGC and precursor glass, both optically polished, and the laser writing direction used for fabricating the waveguides. The UV–VIS–NIR optical absorption spectrum was obtained using a spectrophotometer (Agilent - Varian Cary 50). All the measurements were carried out at room temperature.

The Vickers hardness (H_V) was determined by applying an indentation load of 500 g and for 15 s (Future Tech), according to the ASTM C1327-15 protocol. The H_V was calculated by the equation:

$$H_V = 1.854\frac{F}{d^2} \quad (1)$$

Fig. 1. Magnesium Aluminum Silicate (MAS) Transparent glass–ceramic (TGC) (left) and its precursor glass (right) The red arrow shows the direction of the microfabrication process. (For interpretation of the references to colour in this figure legend, the reader is referred to the web version of this article.)

in which, H_V is the Vickers hardness (GPa), F the applied load (N), d the mean lengths of the diagonals of the indentation (m). The Young moduli (E) of parent glass and glass-ceramic were determined using a sound propagation technique (Sonelastic, ATCP Engenharia Física) in pieces of 25 × 4 × 2.5 mm.

Crystal phase identification was performed by commercial X-ray diffractometer (XRD) equipped with a graphite mono-chromatized Cu-Kα radiation (λ = 1.5406 Å) (Rigaku model Ultima IV). The samples were scanned at a scanning rate of 0.02°/s in the 2θ range of 10°-80°. For Rietveld analysis, the scanning rate of 0.005°/s and 1 s count was utilized, using 10 wt% of alumina (Almatis, 99.9%) as standard crystalline material. The TGC microstructure was observed by Transmission Electron Microscopy - TEM (Tecnai G2, FEI Company). The powered sample was dispersed on acetone to avoid aggregation phenomena and dried on carbon grid.

In relation to the microfabrication process, the optical waveguides were produced inside the samples using a commercial extended-cavity Ti:Sapphire laser oscillator (Femtosource™ XL™ 100), with a repetition rate of 5.2 MHz and a ~18-nm (FWHM) spectral bandwidth centered at 800 nm, that produces up to 60 nJ energy pulses with 50 fs of duration. The schematic setup can be seen in Fig. 2(a). The laser beam is delivered by means of a set of dielectric mirrors to the micromachining area. A small portion is sent to an autocorrelator to measure the laser pulse time duration, which can be adjusted by translating a prism pair in the compressor (scheme not shown), useful to pre-compensate the *chirp* induced majorly by the microscope objective and sample. The pulses were tightly focused, at different depths for each waveguide, through a (40×, 0.67-NA, 0.17 mm thickness glass coverslip correction) microscope objective into the sample. The sample is glued in a support, which was translated at a constant speed with respect to the laser beam by a three-dimensional, computer-driven, linear motion system. A CCD camera is used to both observe the fabrication in real time and image the laser collimated back-reflection when the beam is focused exactly on the sample surface (for alignment purposes). The pulse energy can be adjusted a set of a polarizer preceded by a half waveplate placed along the laser path. A mechanical shutter synchronized with the motion stages allows for fast laser blocking (OFF) and opening (ON) during the fabrication process. Waveguides were written along the entire 4.5- and 7.5-mm length of the MAS TGC and its glass parent samples, respectively, and spaced by 100 μm to prevent crosstalk between them. After micromachining, the ends of both samples were polished to allow coupling of light into the waveguides. The final length of the waveguides was around 4 mm (MAS TGC) and 7 mm (glass). Fig. 2(b) shows an illustration of the experimental setup for coupling light in the waveguide. Before reaching the first microscope lens (10×, 0.25-NA), the HeNe (632.8 nm) laser beam was expanded by a telescope (not shown). The light transmitted through the waveguide was collected by a 20 × microscope objective (0.40-NA) at the exit. Additionally, an iris was used to block any scattered light at the exit of the second objective lens. The exit of the waveguide was imaged on a CCD camera to analyze the guided mode. To determine the insertion loss of the fabricated waveguides, we measured the laser beam power before and after the coupling system, considering all transmission factors of the system. Both femtosecond laser writing as coupling measurements were carried out at Photonics Group (IFSC/USP).

Unpolarized Raman spectra were recorded on a T64000 Horiba Jobin-Yvon spectrometer equipped with a CCD detector and with a microprobe under a 50X long working-distance objective. The 532 nm line of a CW laser operating at 2 W was used as the exciting source. The integration time was 50 s and all spectra were recorded between 30 and 1600 cm^{-1}. The resolution in the spectra is about 1 cm^{-1}. The spot size is 0.6 μm.

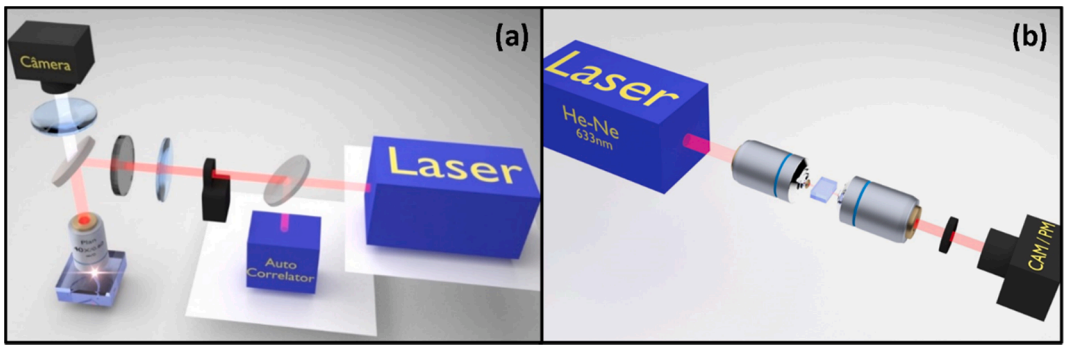

Fig. 2. Micromachining (a) and waveguide coupling (b) systems.

3. Results and discussion

The UV–VIS-NIR optical absorption spectra of both samples (MAS glass–ceramic and glass) are shown in Fig. 3. There is a low absorption around 800 nm for both samples, wavelength used for the waveguide fabrication with fs-pulses. Also, at 632.8 nm, wavelength in which the produced waveguides were tested, the absorption of both samples is almost the same, a little higher for MAS TGC sample. The MAS TGC absorption spectrum shows the typical curve when light scattering is present. In fact, being an inhomogeneous medium with nano(micro)-size crystals (as we will show later), there is appreciable light scattering. Our results show that the wavelength dependence of the scattering coefficient is described by a power law with a constant exponent ($-p$), as for most glass-ceramics [24]. In our case, $p = 5.6 \pm 0.1$ in the spectral range of 360–800 nm. In practice, nonetheless, our laser light, at 800 nm, barely experiences this scattering feature, as can be observed on the inset of Fig. 3. However, despite the scattering losses, the crystallization process resulted in a glass–ceramic having a reasonably high transmittance through a significant portion of the visible and near IR. The measurements were taken for a 4 mm tick glass–ceramic and 7 mm tick precursor glass, both optically polished.

The XRD-pattern of the thermally annealed colorless MAS TGC sample is shown in Fig. 4(a). Its main crystal phase is the $MgO.Al_2O_3$ spinel (S), with 27% in weight, obtained by Rietveld Quantitative Analysis. Additional crystal phases are low(β)-quartz-solid solution (20%), zirconia (▽) (12%) and sapphirine (*) (9%) [25]. The present study thus demonstrates that the amount of residual amorphous phase is approximately 32 wt%.

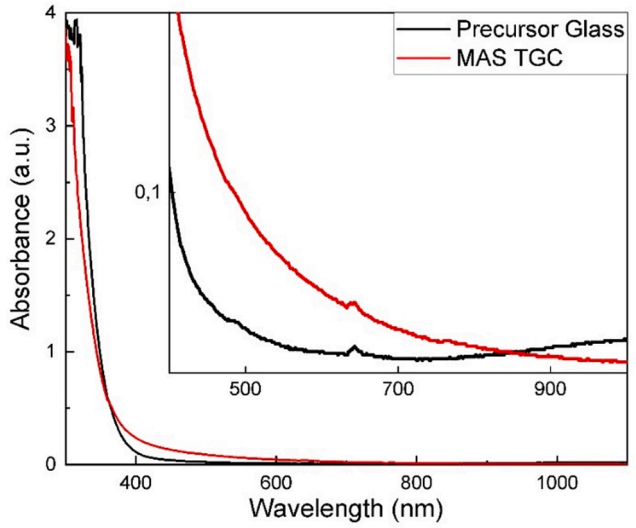

Fig. 3. Optical absorbance from the UV to near-IR of a MAS TGC sample (red line) and the precursor glass (black line) The inset shows a close look. (For interpretation of the references to colour in this figure legend, the reader is referred to the web version of this article.)

To observe the morphology and size of the produced crystals, dark field TEM micrographs were taken and analyzed. Typical crystals are shown at Fig. 4(b). Their shapes are not well defined, whereas their range spans from hundreds of nanometers to a few microns.

After the characterization procedure, waveguides were fabricated in the MAS TGC and its parent sample. The fs-laser beam was focused into the 4-mm-thick polished samples with a 40X microscope objective (0.67NA, 0.17 mm thickness glass coverslip correction), as mentioned before. Firstly, we characterized some specimens to find the threshold pulse energy for heat diffusion, which is clearly determined by the plasma emission, as will be seen later, as a function of depth (Fig. 5). We scanned the sample at a low speed (50 $\mu m/s$), in which we observed variations in the collected spectra in real time. The laser pulse time duration was set to maximize the plasma emission, collected at the side of the sample by a lens and fiber set and directed to a spectrometer, with an integration time of 50μs (schematic not shown). Furthermore, from the geometry of a ray passing through a plane surface [26], the microfabrication depth indicates that the refractive index of the samples are, on average, (1.65 ± 0.3) and (1.52 ± 0.02) for the MAS TGC and the glass, respectively.

Using the plasma emission pattern as a threshold for the heat diffusion is simpler than other methods, such as the 2-fold waveguide diameter increase over the diameter produced by diffusion in a single-pulse interaction [27]. This technique can be useful in the future, due to the fact that good optical waveguides, i.e., the ones that yields the lowest losses, are produced with energies above this threshold. It was not possible to achieve the heat diffusion limit at around 50μm and 250μm below the surface for the TGC, due to power pulse limits of the system. Nonetheless, we observed that the pulse energy required for heat diffusion in the MAS glass–ceramic sample is approximately 2-fold greater than for its precursor glass for each depth. This difference could be explained by two possible reasons. (i) the crystallites embedded in the glass matrix certainly scatters light, therefore one needs higher pulse energy to induce the breakdown and, consequently, the threshold for heat diffusion. However, we demonstrated that the scattering at the writing wavelength is negligible. (ii) the crystal phases obtained changed the local nonlinear refractive index in a way that becomes difficult to achieve multi-photon absorption. Moreover, the pulse duration, which strongly influences the spatial distribution of the energy density in the focal volume due to energy depletion, self-focusing and plasma defocusing [28], were corrected, using a prism pair, for obtaining maximum plasma intensity for each sample. Furthermore, the results showed that the pulses had to be pre-chirped twice as much for the MAS TGC, which indicates a higher material dispersion.

As mentioned previously, the plasma emission can be used to determine the heat diffusion threshold. Fig. 6(a) shows the image collected by the camera used in the microfabrication system for the MAS TGC sample (the precursor glass presents similar results). As can be

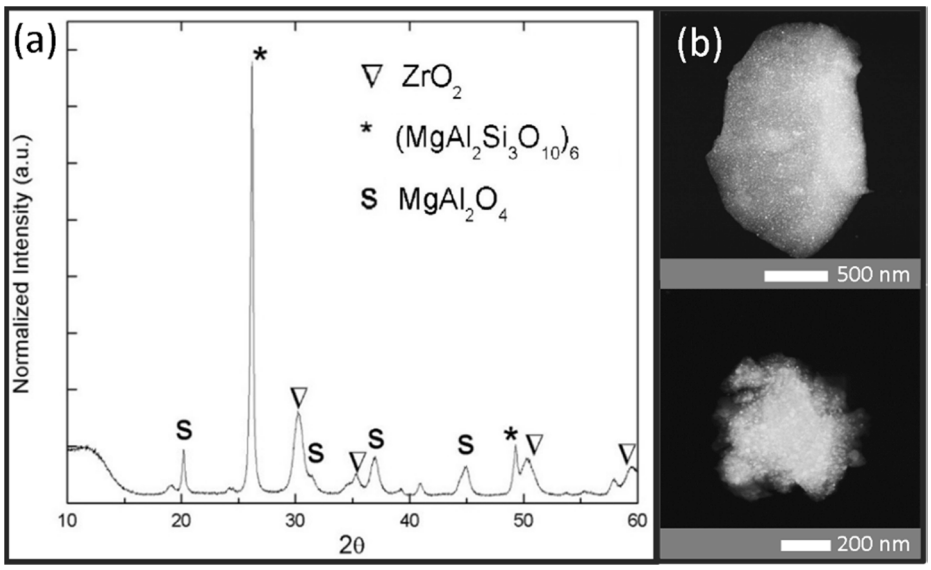

Fig. 4. (a) XRD of the MAS transparent glass-ceramic. (b) Dark field TEM micrograph of the typical crystals in the MAS glass-ceramic, which range from 100 nm to 1 μ m.

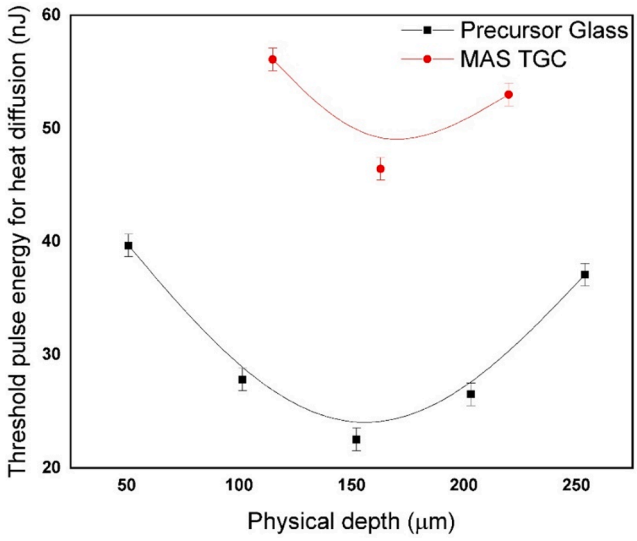

Fig. 5. Threshold pulse energy for heat diffusion as a function of depth for the precursor glass (black squares) and MAS TGC (red circles). Both black and red lines are placed just to guide the eyes. (For interpretation of the references to colour in this figure legend, the reader is referred to the web version of this article.)

observed, the up (above heat diffusion threshold) and the bottom (below heat diffusion threshold) images are dramatically different. The plasma emission suddenly becomes brighter and stronger when the pulse energy reaches the threshold, with no observable state between these two, i.e., it is a dual process only. These two breakdown situations were already reported in the literature [29,30]. The waveguide cross-section (Fig. 6 (b)) of each case is also quite distinct. Fig. 6(c) shows the plasma spectrum obtained for the MAS TGC. It was not possible to record the plasma emission for energies below the threshold (below noise).

To produce the waveguides for testing the guiding properties in both materials, the microfabrication depth was set at 165 μm (152 μm) below surface for the MAS TGC (parent glass), i.e., the lowest pulse energy required to achieve the threshold for heat diffusion. The writing velocity was 500 $\mu m/s$. The waveguide's diameter ranges from 1.63 μm (23 nJ) to 3.15 μm (31 nJ) for the precursor glass; and from 1.87 μm (48 nJ) to 2.27 μm (54 nJ) for the MAS TGC. After the microfabrication process, to be able to launch light into the fabricated waveguides, we optically polished the input and output faces of the sample both samples. After initial alignment, light from a HeNe laser beam (632.8 nm) was coupled into the waveguides. The typical near-field intensity distribution at the output of the waveguides produced in both samples, highest output power, is shown in Fig. 7. A round intensity distribution is observed in Fig. 7(a) for the precursor glass. For the MAS TGC, on the contrary, the intensity distribution is confined to the microscope objective's 3D voxel limit, as can be seen in Fig. 7(c). To estimate the insertion loss ($IL_{dB} = -10 \cdot \log(P_{out}/P_{in})$), we measured P_{in}(laser beam power measured before the entrance lens) and P_{out} (laser beam power measured after the exit lens) of the coupling system, considering all transmission factors. The produced waveguides present an IL of 6.3 dB for the glass, and 8.5 dB for the MAS TGC, on average, which can be certainly improved by exploring other laser capabilities, such as inscription wavelength, focusing, writing speed and other variables [31].

Considering the different results obtained, we measured the Raman spectra of the bulk and in the waveguide core cross section. It is known that the spectra for glasses typically consist of a number of bands, which are often overlapped, that can be assigned to vibrations of different types of bonds [31]. The lack of long-range order in the glass leads to a wide distribution of bond-lengths and -angles compared to crystals of the same composition and, as a consequence, Raman bands in glass are much broader than those in crystals. In fact, when one observes the Raman intensity (Fig. 8) of the precursor glass (black line) and the MAS TGC (red line), there is a clear narrowing of some bands, revealing and corroborating the crystallization of the sample. In order to discuss the modes, it is convenient to discriminate three regions in the Raman spectra. In the low-frequency region (200–700 cm^{-1}), the Raman spectrum of the glass exhibits a major band at 90 cm^{-1} with an asymmetric component to higher frequency at 450 cm^{-1}. This spectrum is similar to those observed previously for other glasses with high silica content [32,33], and the bands are generally associated with motions of bridging oxygens in T-O-T linkages (T = Si, Al). On the other hand, the MAS TGC shows characteristic peaks of its crystal phases. The narrow bands at ~ 142, ~265, ~311, ~452 and ~ 640 cm^{-1} are assigned to tetragonal ZrO_2 [34]. For all the samples, the mid-frequency region (700–900 cm^{-1}) shows a distinct peak near 800 cm^{-1}. This band is usually ascribed to cage motion of Si-O stretching vibrations [6,32,33] and indicates that the crystallization process (red curve) was not total.

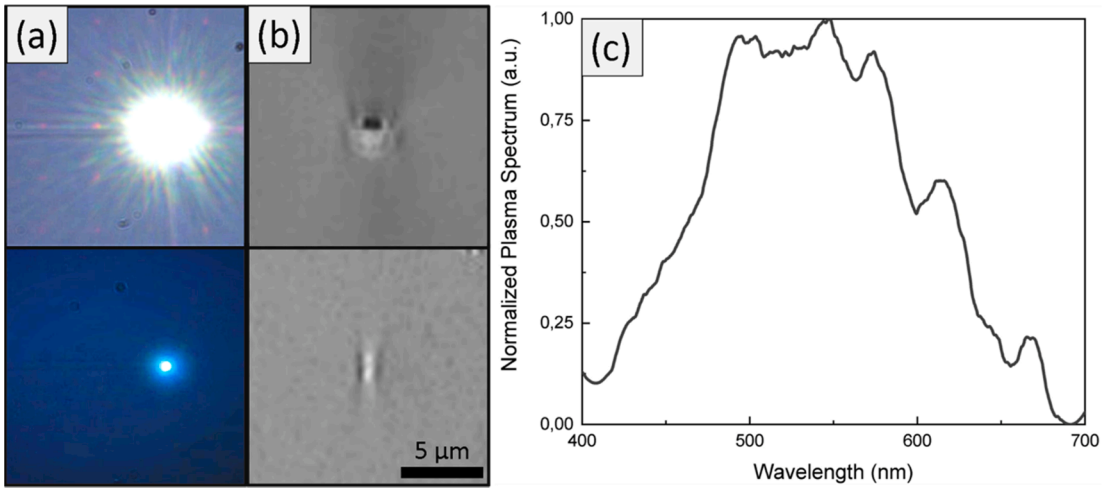

Fig. 6. (a) Image of the microfabrication process in real time obtained by the system camera. (b) Waveguide cross-section at the lateral surface. The top and bottom images are for above and below the threshold energy for heat diffusion. (c) Plasma spectrum recorded for pulse energies above threshold.

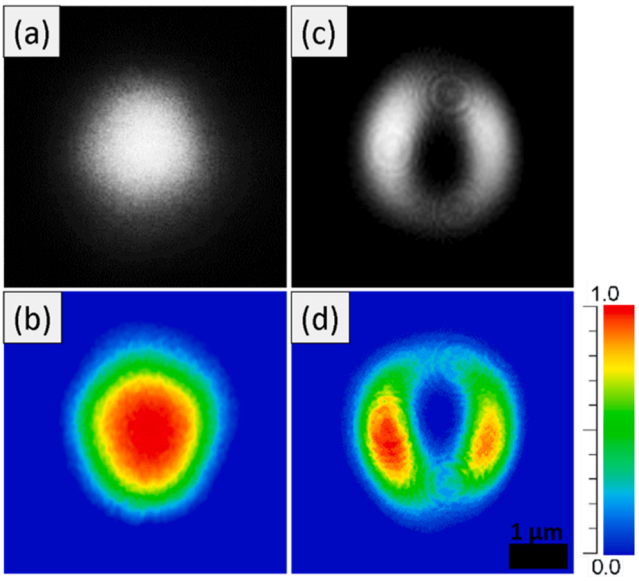

Fig. 7. Near-field intensity distribution at the output of the waveguides produced in the glass (a and b) and in the MAG TGC (c and d).

Finally, the high-frequency region (900–1300 cm^{-1}) shows a broad band centered in 950 cm^{-1} for the black and blue lines, but one can also notice two bands in the bulk MAS TGC (red curve). This result indicates that these two bands are overlapped when amorphization is predominant. In spite of that, Raman modes in this region are ascribed to the symmetric and asymmetric stretching vibrations of the fully polymerized tetrahedral network units, corresponding to the Si(OAl)*y* units. Here, *y* denotes the number of AlO_4 tetrahedra connected to a SiO4 tetrahedron [35] or to (Si,Al)-NBO (non-bridging O atoms) and (Si,Al)-BO (bridging O atoms) stretch bands.

It is interesting to note that the femtosecond microfabrication induced a partial amorphization (blue line). The destruction of crystalline phases is generally associated to a decreasing of the local density and thus the refractive index in the modified region, which could prevent light guiding. Nonetheless, we were able to couple and guide light into the fabricated waveguide. One possible reason could be a slight increase of the effective refractive index in the guiding region. This is possible considering that the writing procedure causes the destruction of the crystalline phases only at the focus spot center, i.e., approximately

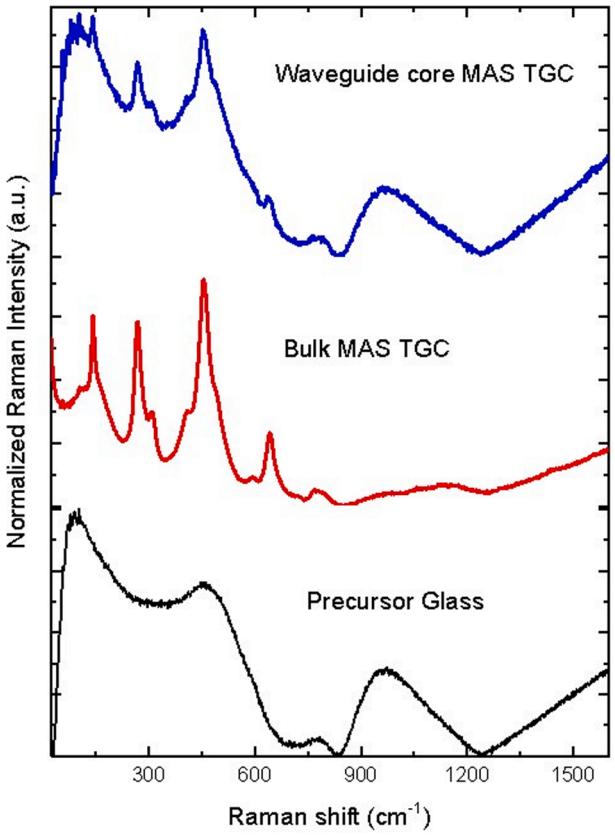

Fig. 8. Raman spectra of the glass (black), MAS TGC (red) and from the produced waveguide inside the transparent glass-ceramic (blue). (For interpretation of the references to colour in this figure legend, the reader is referred to the web version of this article.)

within beam waist (w_0) and Rayleigh range (z_R) of the microscope objective. The waveguide fabricated inside the MAS glass sample does not reveal any difference from the Raman signal obtained on the non-fabricated surface (data not show), which is also noticed in other glass micro-structured by femtosecond laser in this energy range [36].

4. Conclusion

We presented results on the fabrication of optical waveguides inside a MAS transparent glass-ceramic, and in its parent glass using a high energy MHz repetition rate femtosecond laser oscillator. Our glass-ceramic has a hardness and elastic modulus higher than the glasses commonly applied in security windows, and both materials present low absorption in the visible.

We obtained good quality optical waveguides in both materials. In particular, we observed through μRaman experiments that the femtosecond pulse laser action over the MAS TGC sample produces partial amorphization on the fabricated waveguide. This study indicates that glass-ceramics are promising candidates in break-resistance required situations and warrant further studies to replace ordinary glasses in strengthened photonics applications.

Declaration of Competing Interest

The authors declare that they have no known competing financial interests or personal relationships that could have appeared to influence the work reported in this paper.

Acknowledgements

We thank André Romero for assistance in constructing the controllable micromachinign system. We also thank Dr. Benjamin J. A. Moulton and Prof. Dr. Paulo S. Pizani for providing the μRaman measurements. Financial support from FAPESP / São Paulo Research Foundation (Processes number: CEPID 2013/00793-6, 2018/11283-7), CNPq (Conselho Nacional de Desenvolvimento Científico e Tecnológico), CAPES (Coordenação de Aperfeiçoamento de Pessoal de Nível Superior) are acknowledged. This study was financed in part by the Coordenação de Aperfeiçoamento de Pessoal de Nível Superior - Brasil (CAPES) - Finance Code 001.

References

[1] X. Liu, et al., Transparent glass-ceramics functionalized by dispersed crystals, Prog. Mater. Sci. 97 (2018) 38–96.
[2] L.S. Gallo, et al., Transparent glass-ceramics for ballistic protection: materials and challenges, J. Mater. Res. Technol.-Jmr&T 8 (3) (2019) 3357–3372.
[3] G.H. Beall, D.A. Duke, Transparent glass-ceramics, J. Mater. Sci. 4 (4) (1969) 340–352.
[4] J. Deubener, et al., Updated definition of glass-ceramics, J. Non-Cryst. Solids 501 (2018) 3–10.
[5] G.H. Beall, L.R. Pinckney, Nanophase glass-ceramics, J. Am. Ceram. Soc. 82 (1) (1999) 5–16.
[6] T. Benitez, et al., Development of magnesium-aluminum-silicate glass-ceramics nucleated with Nb2O5, Int. J. Appl. Glass Sci. 11 (1) (2020) 155–169.
[7] S. Guddala, et al., Glass-Ceramic waveguides: Fabrication and properties, in: 2010 12th International Conference on Transparent Optical Networks, 2010.
[8] O. Dymshits, M. Shepilov, A. Zhilin, Transparent glass-ceramics for optical applications, MRS Bull. 42 (3) (2017) 200–205.
[9] J. Wang, et al., Integrated photonic quantum technologies, Nat. Photon. (2019).
[10] F. He, et al., Femtosecond laser fabrication of monolithically integrated microfluidic sensors in glass, Sensors 14 (10) (2014) 19402.
[11] K. Minoshima, et al., Photonic device fabrication in glass by use of nonlinear materials processing with a femtosecond laser oscillator, Opt. Lett. 26 (19) (2001) 1516–1518.
[12] A.M. Streltsov, N.F. Borrelli, Fabrication and analysis of a directional coupler written in glass by nanojoule femtosecond laser pulses, Opt. Lett. 26 (1) (2001) 42–43.
[13] K. Yamada, et al., In situ observation of photoinduced refractive-index changes in filaments formed in glasses by femtosecond laser pulses, Opt. Lett. 26 (1) (2001) 19–21.
[14] M. Will, et al., Optical properties of waveguides fabricated in fused silica by femtosecond laser pulses, Appl. Opt. 41 (21) (2002) 4360–4364.
[15] W. Watanabe, et al., Wavelength division with three-dimensional couplers fabricated by filamentation of femtosecond laser pulses, Opt. Lett. 28 (24) (2003) 2491–2493.
[16] T. Shih, et al., Faraday rotation in femtosecond laser micromachined waveguides, Opt. Express 15 (9) (2007) 5809–5814.
[17] Y. Nasu, M. Kohtoku, Y. Hibino, Low-loss waveguides written with a femtosecond laser for flexible interconnection in a planar light-wave circuit, Opt. Lett. 30 (7) (2005) 723–725.
[18] A.M. Kowalevicz, et al., Three-dimensional photonic devices fabricated in glass by use of a femtosecond laser oscillator, Opt. Lett. 30 (9) (2005) 1060–1062.
[19] L. Eldada, L.W. Shacklette, Advances in polymer integrated optics, Selected Topics Quantum Electron., IEEE J. 6 (1) (2000) 54–68.
[20] K.M. Davis, et al., Writing waveguides in glass with a femtosecond laser, Opt. Lett. 21 (21) (1996) 1729–1731.
[21] B.H. Cumpston, et al., Two-photon polymerization initiators for three-dimensional optical data storage and microfabrication, Nature 398 (6722) (1999) 51–54.
[22] S. Maruo, O. Nakamura, S. Kawata, Three-dimensional microfabrication with two-photon-absorbed photopolymerization, Opt. Lett. 22 (2) (1997) 132–134.
[23] D.S. Correa, et al., Femtosecond laser in polymeric materials: microfabrication of doped structures and micromachining, Selected Topics Quantum Electron., IEEE J. 18 (1) (2012) 176–186.
[24] M.P. Shepilov, O.S. Dymshits, A.A. Zhilin, Light scattering in glass-ceramics: revision of the concept, J. Opt. Soc. Am. B 35 (7) (2018) 1717–1724.
[25] M. Dittmer, C. Rüssel, Colorless and high strength MgO/Al2O3/SiO2 glass–ceramic dental material using zirconia as nucleating agent, J. Biomed. Mater. Res. B Appl. Biomater. 100B (2) (2012) 463–470.
[26] G.R. Fowles, Introduction to Modern Optics, ed. N. York., Dover Publication Inc., 1989.
[27] S.M. Eaton, et al., Transition from thermal diffusion to heat accumulation in high repetition rate femtosecond laser writing of buried optical waveguides, Opt. Express 16 (13) (2008) 9443–9458.
[28] J. Burghoff, et al., Structural properties of femtosecond laser-induced modifications in LiNbO3, Appl. Phys. A 86 (2) (2007) 165–170.
[29] C.W. Carr, et al., Radiation produced by femtosecond laser–plasma interaction during dielectric breakdown, Opt. Lett. 30 (6) (2005) 661–663.
[30] W.J. Reichman, et al., Spectroscopic characterization of different femtosecond laser modification regimes in fused silica, J. Opt. Soc. Am. B 24 (7) (2007) 1627–1632.
[31] R. Osellame, G. Cerullo, R. Ramponi, Femtosecond Laser Micromachining - Photonic and Microfluidic Devices in Transparent Materials, Springer, Berlin, Heidelberg, 2012.
[32] D.R. Neuville, et al., Amorphous materials: Properties, structure, and durability†: Structure of Mg- and Mg/Ca aluminosilicate glasses: 27Al NMR and Raman spectroscopy investigations, Am. Mineral. 93 (11–12) (2008) 1721–1731.
[33] A.K. Yadav, P. Singh, A review of the structures of oxide glasses by Raman spectroscopy, RSC Adv. 5 (83) (2015) 67583–67609.
[34] I. Alekseeva, et al., Phase transformations in NiO and CoO doped magnesium aluminosilicate glasses nucleated by ZrO2, Glass Technol. 46 (2) (2005) 187–191.
[35] P. McMillan, B. Piriou, A. Navrotsky, A Raman spectroscopic study of glasses along the joins silica-calcium aluminate, silica-sodium aluminate, and silica-potassium aluminate, Geochim. Cosmochim. Acta 46 (11) (1982) 2021–2037.
[36] J. Hernandez-Rueda, et al., The influence of femtosecond laser wavelength on waveguide fabrication inside fused silica, Appl. Phys. Lett. 110 (16) (2017), 161109.